Geophys. J. Int. (2006) **164,** 441–448 doi: 10.1111/j.1365-246X.2006.02847.x

Uppermost inner core attenuation from PKP data observed at some South American seismological stations

Marian Ivan,[1] Vasile Marza,2* Daniel de Farias Caixeta[2] and Tassia de Melo Arraes[2]

[1]*Department of Geophysics, University of Bucharest,* 6 *Traian Vuia str.,* 70138 *Bucharest o.p.*37, *Romania. E-mail: ivam@gg.unibuc.ro (MI)*
[2]*University of Brasilia, Institute of Geosciences, Seismological Observatory,* 70910-900 *Brasilia-DF, Brazil*

Accepted 2005 October 14. Received 2005 July 19; in original form 2005 March 15

SUMMARY

Q_P factor at the top of the inner core (IC) is derived using the amplitude spectral ratio (PKPbc versus PKPdf) method applied to the waveforms of suitable, strong (magnitude >6.0) intermediate depth and deep ($h > 150$ km) earthquakes recorded at some selected South American stations. In most cases, the sampled volume of the IC is centred beneath the Pacific Ocean, but some Q_P values correspond to volumes under South Africa and under Northern Atlantic. The obtained value of Q_P is 323 $\pm$ 16 (at 95 per cent confidence level), close to a normal (Gaussian) distribution. The maximum depth of penetration of the PKPdf phase into the IC is roughly 333 km, suggesting a possible increase of Q_P with depth, although the large scatter in data prevents a definite conclusion. As regards the geographical patterns no variation was observed.

Key words: amplitude spectral ratio, inner core, Pacific Ocean, PKP-phases attenuation, Q_P factor, South America.

GJI Seismology

1 INTRODUCTION

The attenuation of high-frequency *P* waves in the inner core (IC) has been extensively studied over the last three decades, providing constraints on the core structure and nature (e.g. Helffrich *et al.* 2002). Various studies on traveltimes (e.g. Souriau *et al.* 2003; Xu & Song 2003) suggest heterogeneity, anisotropy or differential rotation of the IC. However, the radial and geographical variations of the IC quality factor Q_P, or its frequency dependency, are still poorly resolved because of uneven sampled area(s), most of the results being restricted to small number of processed events or to uneven distribution of earthquakes and recorders (e.g. Tseng *et al.* 2001). For example, Doornbos (1974) reported Q_P values in the range 200 $\div$ 600, increasing with depth below the IC boundary and frequency independent in the band 0.2–2 Hz, whereas Cormier (1981) obtained a value of 280, constant with depth. Niazi & Johnson (1992) reported Q_P of 176 ($\pm$10), compatible with a depth variation but not confidently resolvable. On the other hand, Tseng *et al.* (2001) reported a lateral variation of the attenuation from 305 ($\pm$25) in Western Pacific to 160 ($\pm$34) in Eastern Pacific areas and an increasing of Q_P with depth from 241 ($\pm$22) for depths less than 210 km to 337 ($\pm$47) for depths greater than 270 km. For paths from southwest Pacific to Western Europe, Souriau & Roudil (1995) observed an exception from linearity of the spectral ratio. Using Romanian network, Ivan & Popa (2004) obtained an average Q_P of 295 $\pm$ 20 (95 per cent confidence level) for a sampled region of the IC centred beneath the Japan Sea. The maximum depth of penetration of the PKPdf phase was roughly 254 km and the data suggest a slight increase of Q_P with depth, although not resolvable, given the data scattering. Bhattacharyya *et al.* (1993) assumes Q_P is frequency independent and constant with depth, while Helffrich *et al.* (2002) obtained no trend with the depth in the range 140–340 km below IC boundary, with Q_P values 130^{+225}_{-52} in a restricted area of the IC lying under Alaska.

In fact, Q_P values exhibit considerable scattering (Bhattacharyya *et al.* 1993; Helffrich *et al.* 2002), possibly associated with strong heterogeneity at the base of the mantle (Bowers *et al.* 2000) or to a mosaic structure of the uppermost part of the Earth's IC (Krasnoshchekov *et al.* 2005). For the time being it makes difficult to resolve frequency dependency, depth dependence or geographical variations, if any. Therefore, a large number of Q_P estimations are necessary in order to improve the statistics and to resolve the above features of the attenuation in the IC.

With respect to most of the earthquakes located in the Western Pacific, the seismological stations in South America are placed at distances around 150°, representing a best location for studies on the IC attenuation. The core phases like PKPdf, PKPbc and PKPab are properly observed, especially for strong, (intermediate) depth events. PKPdf wave penetrates ~300 km deep into the IC, having high attenuation (i.e. very low Q_P values). PKPbc wave has a similar path to PKPdf through the crust and mantle, however, its turning point remains inside the outer core, characterized by a low attenuation (i.e. very high Q_P values), up to a distance around 155° where it starts to be diffracted by the IC boundary. Consequently,

*On leave from Seismological Laboratory, National Institute for Earth Physics, Bucharest, Romania.

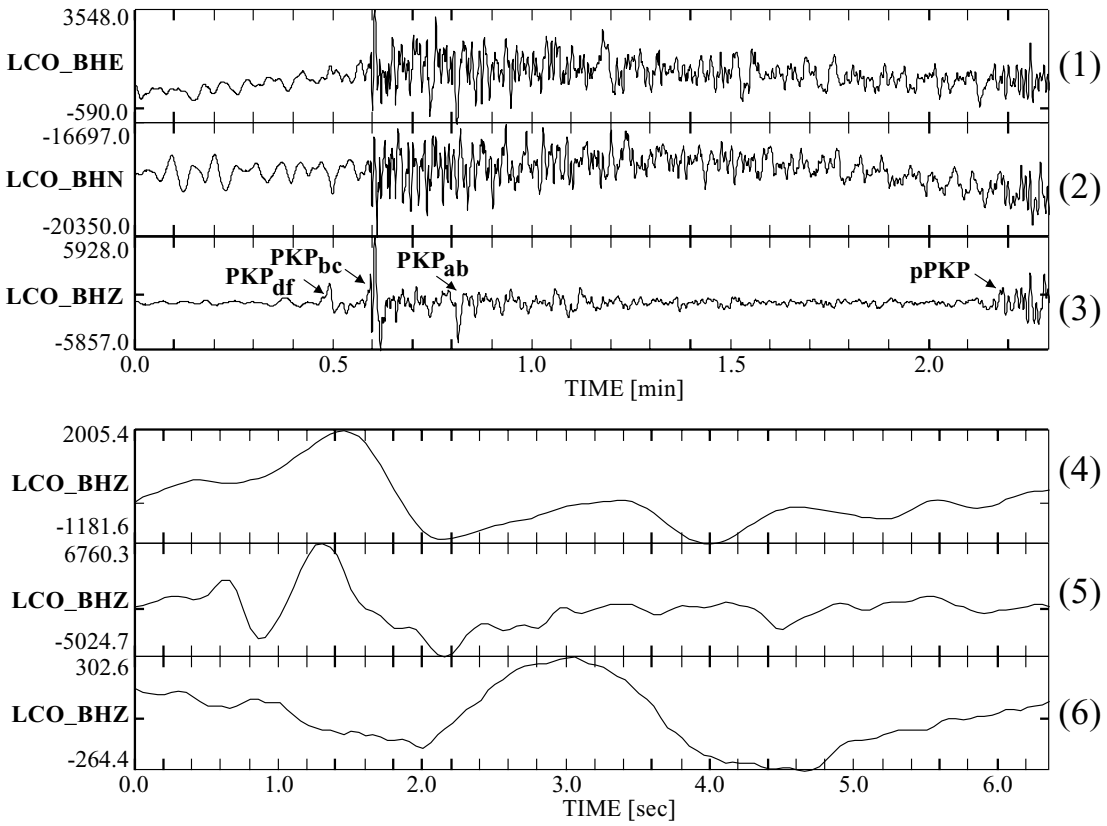

Figure 1. Recording at Las Campanas Astronomical Observatory (LCO) station ($\Delta = 152.3^\circ$) of 2000 October 27 earthquake (broad-band instrument) (traces 1–3). Traces (4) and (5) are the time windows of 128 points immediately following the arrivals of PKPdf and PKPbc, respectively, of the trace (3). Note the depleting in high frequencies of PKPdf phase with respect to PKPbc, assumed to be a result of the attenuation in the IC. The bottom trace (6) is a noise window considered for reference.

PKPdf routinely displays a very emergent arrival, with small amplitudes depleted in high frequencies in contrast with the high amplitude, impulsive onset of the PKPbc phase (e.g. Fig. 1). By using the standard spectral ratio method (e.g. Souriau & Roudil 1995; Helffrich *et al.* 2002 etc.), this pair of phases provides the possibility to investigate the attenuation properties at the top of the IC. In this paper, a total of 83 values of the quality factor Q_P are obtained from 37 major earthquakes ($M_w \geq 6$) in Western Pacific area, recorded at some permanent or temporary South American seismological stations. The recordings belong to the time interval 1994 July 13 to 2004 November 7. All stations are equipped with broad-band sensors. For BDFB, LPAZ and PLCA stations, short-period records are available, as well. The hypocentral data of and additional information on the processed events are summarized in Table 1 and the used stations are shown in Figs 2 and 3.

2 SPECTRAL RATIO METHOD

The amplitude spectrum of a certain wave is the product of the source factor, of the source-to-receiver path and of the instrument response. The source factors corresponding to the PKPdf phase (having a take-off angle $i \sim 9^\circ$ for a deep earthquake recorded at a distance of $\sim 150^\circ$ like event #13 from Table 1) and to the PKPbc branch ($i \sim 14^\circ$) are supposed to differ by a constant only, assuming no significant variation of the attenuation at the source with the take-off angle. That assumption is supported by various studies of the attenuation in the source (e.g. Flanagan & Wiens 1998; Roth *et al.* 1999). The instrument responses for PKPdf and PKPbc are equal, especially for broad-band sensors. Considering the source-to-receiver path effects, it is routinely assumed that the amplitude spectrum of a wave phase decreases exponentially with the frequency f, according to

$$A(f) = A_0 \exp(-\pi f t^*), \tag{1}$$

where A_0 is a constant and t^* is an attenuation parameter defined by

$$t^* = \int_{\text{ray path}} \frac{dt}{Q}. \tag{2}$$

Considering the PKPdf and PKPbc phases, the logarithm of the ratio of their amplitude spectra will be linearly dependent on the frequency (Niazi & Johnson 1992; Bhattacharyya *et al.* 1993), that is,

$$\ln [A_{DF}(f)/A_{BC}(f)] = C - \pi \left(t^*_{DF} - t^*_{BC}\right) f, \tag{3}$$

where C is a certain constant.

Consider a representative earthquake at 388 km depth recorded at 152.3° (i.e. the event 23 at station LCO in Table 1, whose waveform is represented in Fig. 1), the mantle (descending leg) contribution in eq. (2) is $t^* = 0.3248$ s for PKPdf wave for IASP91 model (Buland & Chapman 1983; Kennett & Engdahl 1991) and 0.3368 s for PKPbc. The values corresponding to the outer core are 0.0092 s

Table 1. The hypocentral parameters of the processed events (Source: NEIC). For each station, the distance (Δ) and azimuth (Az) are indicated together with the radius of the turning point (rTP) and the value of the attenuation factor Q_P. All stations are equipped by broad-band sensors, except BDFB, LPAZ and PLCA where SP sensors are also available.

No	Region	Year	Month	Day	Origin time	Latitude (°)	Longitude (°)	Depth (km)	Mag	Station	Δ (°)	Az (°)	rTP (km)	Q
1	Banda Sea	1994	07	13	11:45:23.36	−7.53	127.77	158	6.8	LPAZ	151.5	147	963	290^{+54}_{-39}
										CRIS	149.9	154	1002	296^{+85}_{-54}
										COLL	150.8	147	978	255^{+51}_{-36}
										CHUQ	150.2	149	993	301^{+69}_{-47}
										SCHO	150.7	156	983	233^{+34}_{-26}
										SICA	150.8	148	979	443^{+84}_{-61}
										YUNZ	150.5	155	988	313^{+2}_{-2}
2	Banda Sea	1994	08	30	19:42:46.51	−6.97	124.11	595	6.2	CHIT	150.9	158	963	456^{+96}_{-68}
										CHUQ	152.4	155	926	456^{+132}_{-84}
										CRIS	151.9	160	941	369^{+22}_{-19}
										CRUZ	152	159	937	308^{+70}_{-48}
										DOOR	151.4	157	952	411^{+17}_{-16}
										HIZO	150.7	155	967	353^{+124}_{-73}
										POOP	152.4	157	928	300^{+24}_{-20}
										SCHO	152.5	162	924	342^{+50}_{-38}
										SICA	153.1	154	910	388^{+107}_{-69}
										TACA	152.1	158	935	254^{+38}_{-29}
3	Java Sea	1994	09	28	16:39:51.67	−5.79	110.35	637	6.6	BDFB	149.6	225	993	230^{+22}_{-18}
4	Java Sea	1994	09	28	17:33:58.21	−5.73	110.36	628	6.0	BDFB	149.7	225	992	239^{+78}_{-47}
5	Java Sea	1994	11	15	20:18:11.31	−5.59	110.19	560	6.5	BDFB	149.6	225	996	227^{+47}_{-33}
										ITIT	153.3	194	904	368^{+30}_{-26}
6	Japan Sea	1995	03	31	14:01:40.08	38.21	135.01	354	6.2	BATO	154.3	49	884	426^{+21}_{-19}
										CHUQ	151.6	51	955	243^{+1}_{-1}
										LAJO	151.7	50	953	236^{+37}_{-28}
										SALI	152.9	53	922	247^{+2}_{-2}
										SICA	151.1	50	965	229^{+14}_{-12}
7	Mariana Isls.	1995	04	08	17:45:12.92	21.83	142.69	267	6.7	BATO	153.6	90	905	515^{+20}_{-19}
										CHUQ	151.1	88	969	354^{+60}_{-45}
										HIZO	151	91	972	415^{+7}_{-6}
										LIRI	150.5	92	984	271^{+12}_{-11}
										POOP	151.9	88	949	305^{+34}_{-28}
										SALI	151.5	91	959	405^{+47}_{-38}
										SICA	151	86	971	403^{+121}_{-76}
8	S. Honshu	1995	07	07	21:15:19.70	33.97	137.13	333	6.0	LPAZ	151.2	58	963	267^{+28}_{-23}
9	Kuril Isls.	1996	02	01	07:18:04.23	44.85	146.27	170	6.2	PLCA	152.9	94	927	344^{+54}_{-41}
10	Solomon Isls.	1996	05	02	13:34:28.99	−4.55	154.83	500	6.6	BDFB	149.7	132	996	274^{+39}_{-30}
11	Bonin Isls.	1996	06	26	03:22:03.14	27.73	139.75	468	6.3	LPAZ	151.8	72	946	250^{+10}_{-9}
										PLCA	152	126	942	258^{+11}_{-10}
12	Mariana Isls.	1996	07	06	21:36:28.72	21.97	142.83	241	6.2	LPAZ	150.3	84	991	222^{+20}_{-17}
										PEL	148.4	118	1033	291^{+29}_{-24}
13	Java Sea	1997	07	11	09:55:12.58	-5.7	110.80	574	6.0	BDFB	150	224	986	207^{+21}_{-18}
14	Volcano Isls.	1998	02	07	01:18:59.50	24.82	141.75	525	6.4	PTGA	148	44	1033	383^{+69}_{-51}
										LPAZ	150.8	79	967	376^{+100}_{-65}
										PEL	150.6	114	973	407^{+128}_{-79}
15	Mariana Isls.	1998	05	15	05:58:06.04	14.18	144.88	154	6.1	LPAZ	148.1	98	1041	280^{+29}_{-24}
16	NW Ryukyu	1998	10	03	11:15:42.69	28.5	127.61	226	6.2	PTGA	151.3	16	990	433^{+153}_{-90}

Table 1. (*Continued*.)

No	Region	Year	Month	Day	Origin time	Latitude (°)	Longitude (°)	Depth (km)	Mag	Station	Δ (°)	Az (°)	rTP (km)	Q
17	Bonin Isls.	1999	01	12	02:32:25.59	26.74	140.17	440	6.0	PLCA	151.1	127	963	297
18	Russia-China	1999	04	08	13:10:34.08	43.61	130.35	565	7.1	BDFB	152	356	938	346^{+27}_{-24}
19	Bonin Isls.	1999	07	03	05:30:10.09	26.32	140.48	430	6.1	PTGA	147.7	41	1042	297^{+14}_{-13}
										PLCA	150.6	127	976	377^{+68}_{-50}
										LPAZ	151.6	75	953	191^{+29}_{-23}
20	Vanuatu Isls.	1999	09	17	14:54:48.72	-13.79	167.24	196	6.3	RCBR	149.8	129	1003	321
21	Okhotsk Sea	2000	07	10	09:58:18.89	46.83	145.42	359	6.1	NP04	150.6	26	980	350^{+75}_{-52}
22	Banda Sea	2000	08	07	14:33:55.91	−7.02	123.36	648	6.5	SPB	148.1	196	1028	291
										NNA	152.3	133	926	354^{+63}_{-47}
23	Bonin Isls.	2000	10	27	04:21:51.60	26.27	140.46	388	6.3	LCO	152.3	103	936	288^{+7}_{-6}
										PEL	152.2	112	939	323
										PLCA	150.6	127	978	298
24	Bali Sea	2001	02	16	05:59:09.48	−7.16	117.49	521	6.1	BDFB	153	212	914	537^{+220}_{-121}
										NP04	149.7	209	996	251^{+31}_{-25}
25	Hindu Kush	2001	02	25	02:21:59.59	36.42	70.88	202	6.2	PLCA	149.8	250	1003	293^{+75}_{-50}
										AMER	149.5	260	1012	269^{+13}_{-12}
										CONS	150.4	261	989	330^{+37}_{-30}
26	Okhotsk Sea	2001	02	26	05:58:22.43	46.81	144.52	392	6.1	CONS	150.5	82	980	301^{+25}_{-22}
27	Mariana Isls.	2001	07	03	13:10:42.60	21.64	142.98	290	6.5	TRQA	153	133	922	423^{+24}_{-22}
										NIEB	148.7	124	1026	283^{+169}_{-77}
										PACH	150.3	113	989	337^{+100}_{-63}
										RINC	151.2	114	966	303^{+23}_{-20}
										USPA	149.4	117	1010	301^{+32}_{-27}
28	Minahassa	2001	12	09	18:15:02.60	0.0	122.87	156	6.1	LCO	148.2	157	1039	472^{+52}_{-43}
29	SE Russia	2002	02	01	21:55:20.99	45.46	136.72	355	6.2	LCO	152.9	62	922	263^{+20}_{-17}
										NP04	153.7	9	902	312^{+8}_{-7}
30	Russia-China	2002	06	28	17:19:30.27	43.75	130.67	566	7.3	BDFB	151.9	357	941	250^{+8}_{-7}
31	NE China	2002	09	15	08:39:32.70	44.83	129.92	586	6.4	BDFB	150.8	356	966	271^{+12}_{-11}
32	Bali Sea	2002	10	03	19:05:10.67	−7.53	115.66	315	6.0	BDFB	151.7	215	955	245^{+44}_{-32}
										NP04	148.4	211	1031	278^{+22}_{-19}
33	Solomon Isls.	2003	06	12	08:59:20.24	-5.99	154.76	186	6.3	MPG	152.7	90	934	350^{+14}_{-13}
34	SE Russia	2003	07	27	06:25:31.95	47.15	139.25	470	6.8	LCO	150.6	63	976	310^{+73}_{-50}
										NP04	151.7	14	950	292^{+43}_{-33}
35	Banda Sea	2003	08	28	06:38:11.63	-7.32	126.05	409	6.0	LPAZ	152.5	149	930	390^{+21}_{-19}
36	S. Honshu	2003	11	12	08:26:43.74	33.17	137.07	384	6.4	RCBR	151.9	345	970	355
										LPAZ	151.7	60	952	324^{+49}_{-38}
37	Okhotsk Sea	2004	11	07	02:02:26.14	47.94	144.48	473	6.2	CPUP	152.5	46	930	471^{+26}_{-24}

and 0.0112 s, while for the mantle and crust (ascending leg), they are 0.401 s and 0.4138 s, respectively. That is, the difference of the attenuation parameters $\Delta t^* = t^*_{DF} - t^*_{BC}$ is around −0.03 s for the crust, mantle and outer core path. In real cases, the Δt^* value estimated from the slope of the regression line according to eq. (3) is around 0.5 s. It follows that the difference is mainly related to the IC path of PKPdf. Consequently, the Q_P values in the IC can been derived through

$$Q_P = \pi \frac{t_{DF}}{S}, \tag{4}$$

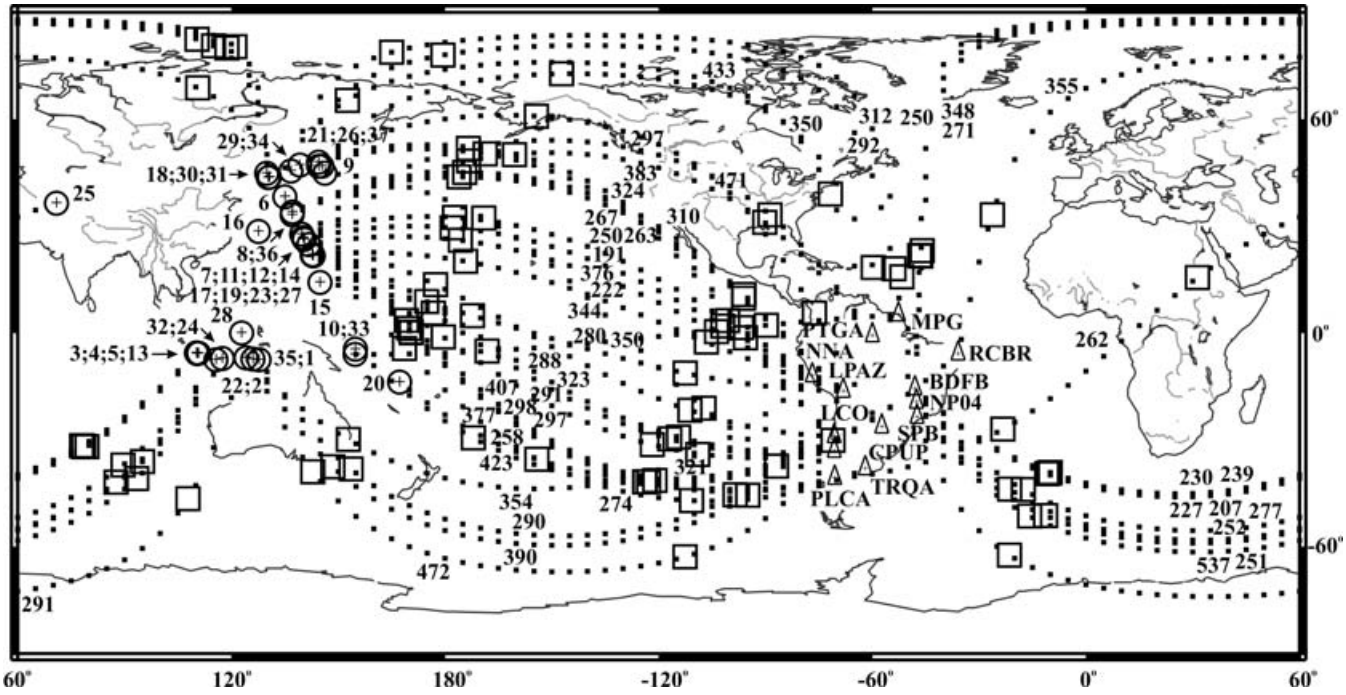

Figure 2. Location of permanent stations (triangles) and epicentres (circles) (see Table 1 for corresponding events). Doted lines show surface projections of the PKPdf rays. Piercing points to the ICB are indicated by squares. Individual Q values are displayed in the proximity of the surface projection of the turning point.

where S is the absolute value of the slope of the regression line described by eq. (3) and t_{DF} is the propagation time of PKPdf phase in the IC.

Several papers discuss in detail the applicability and limitations of the spectral ratio method, mainly from a theoretical point of view (e.g. Bowers *et al.* 2000), but there are cases when the derived attenuation results are not reliable. In fact, use of eqs (3) and (4) assumes both PKPdf and PKPbc waves contain a sufficient amount of energy in the analysed frequency range, routinely [0.2 ÷ 2 Hz]. Some recordings show PKPdf consisting by a monochromatic pulse and/or having the energy focused inside the first 2–3 seconds only of the wave train, this feature could be the result of a slow faulting process or just a radiation effect due to the projections of the PKP rays very close to the nodal planes on the focal hemisphere (Cormier 1981). The contamination of PKPbc by PKPdf (or by its reverberations), or the contamination of both PKP phases by noise can be important too, in some cases. While the last assumption can be satisfactory verified by comparing the wave and noise spectra (supposed to be stationary), the former one could be true for most of the complex rupture earthquakes (multiple events) with two (or more) (strong) events occurring several seconds apart, especially when broad-band recordings are used. Finally, we note that the linearity in eq. (3) is sometimes substantially disturbed by the presence of some narrow absorption peaks present on a single PKP spectrum (more frequently, in PKPbc), possibly associated with strong heterogeneity at the base of the mantle or to the top of the IC (Bowers *et al.* 2000; Krasnoshchekov *et al.* 2005).

3 DATA, PROCESSING METHODOLOGY AND RESULTS

In order to avoid the above-mentioned complications, we have processed only intermediate depth or deep events, in order to minimize scattering of the short-period amplitudes of the PKP phases inside crust or upper mantle and lose of high energy. The investigated earthquakes show a variety of focal mechanisms and focal depths. Check for complex earthquakes was made by visual inspection of the PKPdf wave train and by using International Seismological Centre (ISC) information. The quality factor Q_P is evaluated by using the standard methodology, still no previous filtering or tapering was applied to the signal.

At the beginning of the analysis, 150 broad-band and short-period (where available) data strings have been obtained from the online archive maintained by the Incorporated Research Institutions for Seismology (IRIS). In a limited number of cases, data have been obtained from PIDC AutoDRM. For each processed event, the digital data retrieved by using PITSA software (Scherbaum & Johnson 1992) have been carefully examined and the observed arrival times of the PKP phases have been checked with respect to the prediction given by the IASP91 model. Generally, the (O–C) time residuals do not exceed 3 s, a value slightly smaller when compared to the travel-times predicted by **ak135** velocity model (Kennett *et al.* 1995). The phase polarities with respect to the fault plane solutions reported in ISC Bulletin (routinely, Harvard CMT solutions) have been also considered. After reliable identification of the PKP arrivals, constant windows of 128 points (for the broad-band instrument with sampling rate of 20 Hz) or 256 points (for stations at 40 Hz sampling) have been used to evaluate the natural logarithm of the amplitude spectra. In a very few of cases a small number of zeroes were necessary to be padded to the processed window. A noise window of the same length, preceding the onset of the PKPdf phase has been selected and used as reference. Spectral computation for PKPdf, PKPbc and noise windows has been performed by using the (input bit reversal) FFT subroutine described by Stearns (1975). In almost all cases a clear change of the spectral slope around 2 Hz is observed (viz. Fig. 4). Consequently, the computations were repeated for at least two frequency windows close to 0.2 ÷ 2 Hz frequency range, where

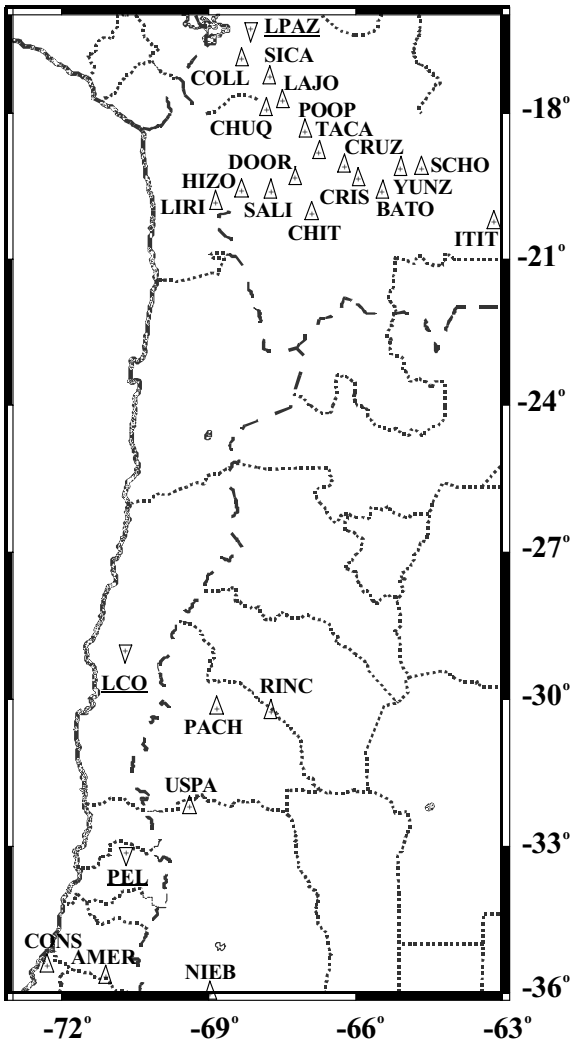

Figure 3. Location of temporary stations used in this study (BB Andean Joint Experiment and Chile Argentina Experiment). Permanent stations in the area (LPAZ, LCO and PEL) are plotted for reference.

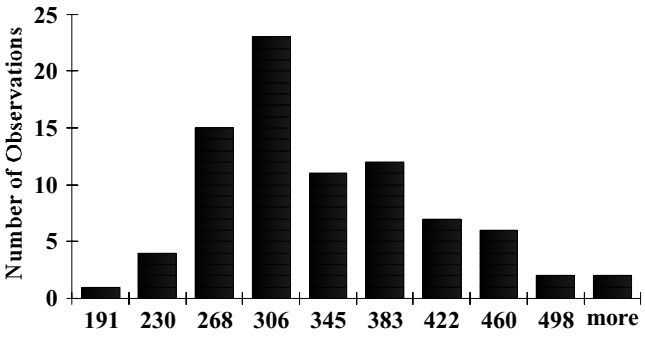

Figure 5. Histogram of Q_P values, showing a distribution close to Gaussian one.

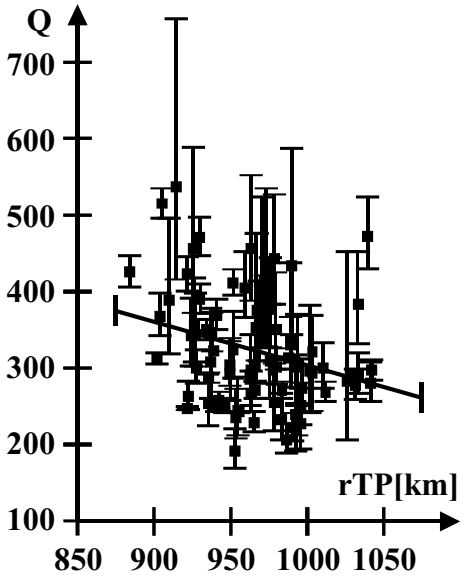

Figure 6. Q_P values versus radius of the turning point of the PKPdf wave. Solid line shows the regression trend.

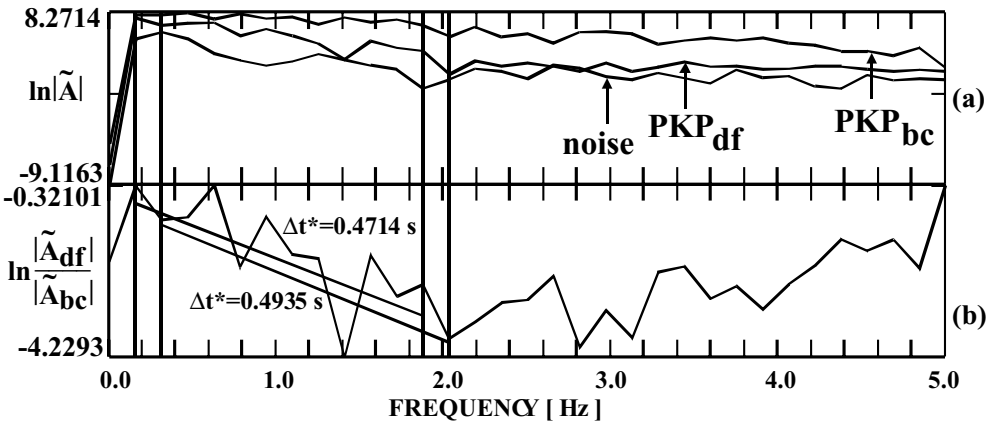

Figure 4. Logarithm of the amplitude spectra for the time windows from Fig. 1 (below 5 Hz). (a) spectra of PKP phases and of the noise; (b) difference DF–BC. Note the linear decreasing below approximately 2 Hz. Values of the attenuation difference $\Delta t^* = t^*_{DF} - t^*_{BC}$ are indicated for the frequency windows 0.156 ÷ 1.875 Hz and 0.312 ÷ 2.031 Hz.

Table 2. Synopsis of some previous inferences on Q_P.

Source	Depth behaviour of Q_P	Q_P range/value	Q_P behaviour in Frequency Band (0.2–2 Hz)
Doornbos (1974)	Variable (increasing with depth below ICB)	200–600	Independent
Cormier (1981)	Constant	≈280	–
Niazi & Johnson (1992)	Compatible with a depth variation but not resolvable	176 (±10)	—
Tseng *et al.* (2001)	Variable	241 (±22) for depths <210 km to 337 (±47) for depths >270 km	Independent
	Geographical variation	Western Pacific 305 (±25) Eastern Pacific 160 (±34)	
Helffrich *et al.* (2002)	No trend with depth	130^{+255}_{-52} (between 140–340 km)	—
Ivan & Popa (2004)	Compatible with a depth variation but not resolvable	295 (±20)	Independent
Present paper	Compatible with a depth variation but not resolvable	323 (±16)	Independent

Note: ICB = inner core boundary.

the amplitude spectra of both PKP waves are clearly above the noise spectrum and display a decreasing linear variation. For each frequency window, a linear regression is fitted to the logarithm of the spectral amplitudes ratio of PKPdf to PKPbc. Finally, the Q_P value is obtained from eq. (4), the propagation time of PKPdf wave in the IC being evaluated by using the **ak135** velocity model (Kennett *et al.* 1995). The computed values of Q_P for various 'source-station' combinations are presented in Table 1 (last column) and the geographical distribution is showed in Fig. 2. In order to assess the overall features and confidence of the results a statistical analysis was subsequently performed.

4 DISCUSSION AND CONCLUSIONS

Computations performed at slightly different frequency windows (e.g. 0.156 ÷ 1.875 Hz or 0.312 ÷ 2.031 Hz) routinely exhibit very similar results (see Fig. 4). Moreover, this aspect is still valid if computations are performed for frequency ranges 0.156 ÷ 0.938, 0.156 ÷ 1.094, ..., 0.156 ÷ 1.719 Hz, or 0.313 ÷ 1.094, 0.469 ÷ 1.25, ..., 1.25 ÷ 2.031 Hz. For the first set of the above windows, data from Fig. 4 give an average $\Delta t^* = 0.4911 \pm 0.153$ s (95 per cent confidence level), while the second set of frequency ranges leads to $\Delta t^* = 0.5159 \pm 0.2909$ s (95 per cent confidence level). In fact, in all cases, the residual spectrum (after removing the linear trend) shows no definite concave/convex shape, suggesting Q_P is frequency independent in the range 0.2÷2 Hz (Bhattacharyya *et al.* 1993). There is also no apparent correlation of Q_P to the type of the recording instrument (broad-band or short-period), especially for low levels of noise on BB recordings. For example, the attenuation differences derived for the 1994 September 28 Java Sea event recorded at BDFB station are $\Delta t^* = 0.614$ s and $\Delta t^* = 0.4952$ s in the frequency ranges 0.156 ÷ 1.875 Hz and 0.312 ÷ 2.031 Hz respectively, for the BB recording. The corresponding values are $\Delta t^* = 0.5074$ s and $\Delta t^* = 0.5684$ s, respectively, for the SP recording. The average value from 83 determinations of Q_P is 323 ± 16 (95 per cent confidence level), with a quasi-normal distribution (Fig. 5), this value is slightly modified to 307 if, instead, Q_P^{-1} is averaged. The obtained average of Q_P is in the range $Q_P^{-1} \in [0.003, 0.004]$, obtained for 0.2 ÷ 2 Hz frequency band by Cormier (1981) using short-period synthesized seismograms. It is also in a good agreement to the previous results using spectral ratio method reported by Helffrich *et al.* (2002), that is, $Q_P \in [78, 385]$, a result derived by averaging Q^{-1}. No geographical variation of the attenuation is confidently observed in our study.

A plot of Q_P values versus the radius of the turning point (r^{TP}; equivalently termed ray vertex) of PKPdf shows a possible increase of Q_P with the depth in the IC (Fig. 6), described by the regression line

$$Q_P = 873.34 - 0.5695 r^{TP}. \quad (5)$$

However, the large scatter in the data ($R^2 = 0.0763$) prevents a clear-cut result from being drawn.

For the sake of convenience we present in Table 2 a synopsis of the results of other investigators regarding the Q_P ranges and its features (depth or frequency dependence, if any, geographical variation, etc.) allowing the reader for making a direct comparison of our results with the previous authors.

ACKNOWLEDGMENTS

The authors express their deep gratitude to Rick Benson, Anh Ngo and other people from IRIS DMC for support in acquiring the input data for this study. The comments of J. Schweitzer and another anonymous reviewer greatly helped to improve the manuscript. GMT files (Wessel & Smith 1996) have been used to prepare some figures.

REFERENCES

Bhattacharyya, J., Shearer, P. & Master, G., 1993. Inner core attenuation from short period PKP(BC) versus PKP(DF) waveforms, *Geophys J. Int.,* **144,** 1–11.

Bowers, D., McCormack, D.A. & Sharrock, D.S., 2000. Observations of PKP(DF) and PKP(BC) across the United Kingdom: implications for studies of attenuation in the Earth's core, *Geophys. J. Int.,* **140,** 374–384.

Buland, R. & Chapman, C.H., 1983. The computation of seismic travel times, *Bull. Seism. Soc. Am.,* **73,** 1271–1302.

Cormier, V.F., 1981. Short-period PKP phases and the anelastic mechanism of the inner core, *Phys. Earth Planet. Inter.,* **24,** 291–301.

Doornbos, D.J., 1974. The anelasticity of the inner core, *Geophys. J.R. astr. Soc.,* **38,** 397–415.

Flanagan, M.P. & Wiens, D.A., 1998. Attenuation of broadband P and S waves in Tonga: observations of frequency dependent Q, *Pure appl. Geophys.,* **153,** 345–375.

Helffrich, G., Kaneshima, S. & Kendall, J.-M., 2002. A local, crossing-path study of attenuation and anisotropy of the inner core, *Geophys. Res. Lett.,* **29,** 1568–1572.

International Seismological Centre, On-line Bulletin Internatl. Seismol. Centre, Thatcham, UK (available at http://www.isc.ac.uk/Bull.

Ivan, M. & Popa, M., 2004. Attenuation in the uppermost inner core from PKP observed at some Romanian stations, *J. Balkan Geophys. Soc.,* **7,** 23–29.

Kennett, B.L.N. & Engdahl, E.R., 1991. Travel times for global earthquake location and phase identification, *Geophys. J. Int.,* **105,** 429–465.

Kennett, B.L.N., Engdahl, E.R. & Buland, R., 1995. Constraints on seismic velocities in the Earth from travel times, *Geophys J. Int.,* **122,** 108–124.

Krasnoshchekov, D.N., Kaazik, P.B. & Ovtchinnikov, V.M., 2005. Seismological evidence for mosaic structure of the surface of the Earth's inner core, *Nature,* **435,** 483–487.

Niazi, M. & Johnson, L.R., 1992. Q in the inner core, *Phys. Earth Planet Inter.,* **74,** 55–62.

Roth, E.G., Wiens, D.A., Dorman, L.M., Hildebrand, J. & Webb, S.C., 1999. Seismic attenuation tomography of the Tonga-Fiji region using phase pair methods, *J. Geophys. Res.,* **104,** 4795–4809.

Scherbaum, F. & Johnson, J., 1992. *Programmable Interactive Toolbox for Seismological Analysis (PITSA)*, IASPEI Software Library, Vol. **5**.

Souriau, A. & Roudil, P., 1995. Attenuation in the uppermost inner core from broad-band GEOSCOPE PKP data, *Geophys J. Int.,* **123,** 572–587.

Souriau, A., Garcia, R. & Poupinet, G., 2003. The seismological picture of the inner core: structure and rotation, *C.R. Geoscience,* **335,** 51–63.

Stearns, S.D., 1975. *Digital Signal Analysis*, Hayden Book Co., Inc., New Jersey.

Tseng, T.L., Huang, B.S. & Chin, B.H., 2001. Depth-dependent attenuation in the uppermost inner core from the Taiwan short period seismic array PKP data, *Geophys. Res. Lett.,* **28,** 459–462.

Wessel, P. & Smith, W.H.F., 1996. A global, self-consistent, hierarchical, high-resolution shoreline database, *J. Geophys. Res.,* **101,** 8741–8743.

Xu, X. & Song, X., 2003. Evidence for inner core super-rotation from time-dependent differential PKP traveltimes observed at Beijing Seismic Network, *Geophys J. Int.,* **152,** 509–514.